

Optical Engineering

SPIEDigitalLibrary.org/oe

Dynamic shape and strain measurements of rotating tire using a sampling moiré method

Motoharu Fujigaki
Kosuke Shimo
Akihiro Masaya
Yoshiharu Morimoto

Dynamic shape and strain measurements of rotating tire using a sampling moiré method

Motoharu Fujigaki

Wakayama University
Faculty of Systems Engineering
Wakayama 640-8510, Japan
E-mail: fujigaki@sys.wakayama-u.ac.jp

Kosuke Shimo

Wakayama University
Graduate School of Systems Engineering
Wakayama 640-8510, Japan

Akihiro Masaya

Wakayama University
Faculty of Systems Engineering
Wakayama 640-8510, Japan

Yoshiharu Morimoto

Moiré Institute Incorporated
Osaka 598-0046, Japan

Abstract. Shape measurements and strain distribution measurements are important for analyzing the behavior of a rotating tire. Recently, a two-dimensional phase analysis method using phase-shifting moiré patterns, which are generated computationally from a two-dimensional grating image, was proposed. This method is well suited to the dynamic shape and strain measurement because the phase can be accurately obtained from a two-dimensional grating image. We show that it is possible to analyze the strain distribution and shape measurements of a moving object using a grating pattern attached to the surface of the specimen, and a dynamic shape and strain measurement system using the sampling moiré method is developed in this paper. The principle of the method and the experimental results of the method when applied to a rotating object are shown.
© 2011 Society of Photo-Optical Instrumentation Engineers (SPIE). [DOI: 10.1117/1.3579525]

Subject terms: shape measurement; strain distribution measurement; sampling moiré method; phase-shifting method; dynamic analysis.

Paper 101068SSPR received Dec. 21, 2010; revised manuscript received Mar. 17, 2011; accepted for publication Mar. 18, 2011; published online Jun. 14, 2011.

1 Introduction

Shape measurements and strain distribution measurements are important in analyzing the behavior of a rotating object. The results can be applied to the computational analysis. The stereoscopic method is often used for measuring three-dimensional (3D) coordinates on the surface of an object. The 3D coordinates are obtained from two images of an object recorded from different directions by two cameras. It is important to accurately locate the corresponding points between the two images, and in particular the accuracy of the 3D coordinates is important when using the coordinates to analyze strain distribution before and after deformation of the object.

As a conventional method, digital image correlation is a well-known method used to find corresponding points between two images using random patterns.^{1,2} This method is when measuring displacement and strain distributions. In the case of a rotating tire, measurement methods using Fourier transform have been proposed.³⁻⁵ These measurement methods have some problems, including the time required for analysis and measurement accuracy.

A spatial fringe analysis method using a sampling technique was proposed by Arai et al.^{6,7} The method is used to analyze the phase distribution of phase-shifted moiré images which are produced computationally from a grating image. The method is useful and accurate. It is often used for electronic speckle pattern interferometry.⁸⁻¹⁰ We applied this method to analyze a two-dimensional (2D) grating image. This method, called a sampling moiré method, was also applied to analyze a deformation measurement.¹¹ The principle of the phase analysis method for one-dimensional grating is essentially the same as the spatial fringe analysis method using a sampling technique. The sampling moiré method applied for a 2D grating image can be used to find

corresponding points between two highly accurate images using regular 2D grating patterns.

The high accuracy of this method is due to the analysis of the phase of the grating pattern using a phase-shifting method with 2D averaging for different grating pitches. The phase-shifting method can be performed with phase-shifted moiré patterns generated computationally from a one-shot grating image. Therefore, this method is suitable for shape and strain distribution measurements of a dynamic 3D object such as a rotating tire.

In this paper, we developed a dynamic shape and strain measurement system for experimental testing using the sampling moiré method. First, experimental results of the strain measurement of a stretched rubber belt are shown to confirm the accuracy of strain measurements with this method. Second, the experimental results of measuring the shape and strain of a rotating tire are shown.

2 Principle of Sampling Moiré Method

2.1 Spatial Fringe Analysis Method Using a Sampling Technique

The principle of the phase analysis method for one-dimensional grating in a sampling moiré method is essentially the same as the spatial fringe analysis method using a sampling technique.^{6,7} In the sampling moiré method, a specimen grating pattern placed on an object is recorded by a digital camera. Though the digitized image only shows the grating, a moiré fringe pattern appears by thinning out the pixels; that is, by sampling the image with a constant pixel pitch. Figure 1 illustrates the appearance of moiré fringe patterns by the sampling moiré method. In Fig. 1, only three horizontal lines are shown. Figure 1(a) shows the deformed grating pattern attached to the specimen. The pitch of the grating in Fig. 1 is 1.125 times larger than that of the sampling points. The recorded image is shown in Fig. 1(b), in which no moiré fringe pattern can be discerned. Figure 1(c)

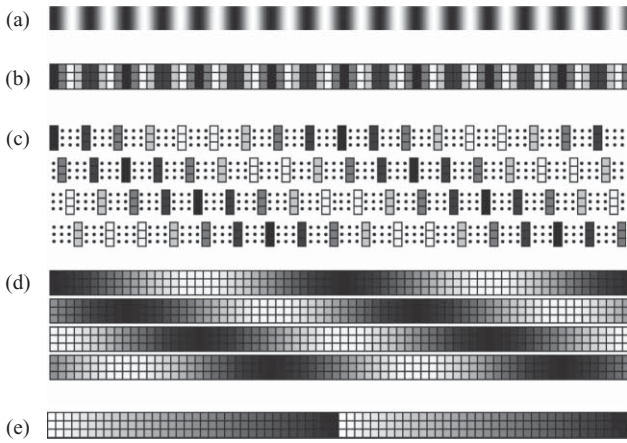


Fig. 1 Principle of the phase-shifting moiré method (a) Deformed grating pattern on specimen. (b) Recorded image by digital camera. (c) Moiré fringe patterns obtained when every N ($= 4$) pixel from the first, second, third, and fourth sampling point is picked up from (b), respectively. (d) Linear interpolated images from (c). (e) Phase θ_m distribution analyzed from Fig. (d).

shows the moiré fringe patterns when the recorded image is sampled at every N th pixel (in Fig. 1, $N = 4$) The four images in Fig. 1(c) are obtained by using the first, second, third, and fourth pixels of Fig. 1(b) as the sampling start point, respectively. This process corresponds to the phase-shifting of the fringe pattern. The sampled images shown in Fig. 1(c) are interpolated using neighboring data. Then, the four phase-shifted moiré images shown in Fig. 1(d) are obtained from a single picture in Fig. 1(b).

The k th phase-shifted images can be expressed approximately as follows:

$$I_k(i, j) = a(i, j) \cos \left[\theta(i, j) + k \frac{2\pi}{N} \right] + b(i, j) \quad (k = 0, 1, \dots, N - 1). \quad (1)$$

Here, $a(i, j)$ represents the amplitude of the grating intensity, $b(i, j)$ represents the background intensity, and $\theta(i, j)$ is the initial phase value. The phase distribution of the moiré pattern can be obtained by the discrete Fourier transform algorithm using Eq. (2) as follows:

$$\tan \theta = - \frac{\sum_{k=0}^{N-1} I_k \sin \left(k \frac{2\pi}{N} \right)}{\sum_{k=0}^{N-1} I_k \cos \left(k \frac{2\pi}{N} \right)}. \quad (2)$$

The phase θ_m of the moiré pattern is defined as the difference between the grating phase θ_g and the phase θ_r of the reference grating (i.e., the sampling phase) as follows:

$$\theta_m = \text{Wrap}(\theta_g - \theta_r). \quad (3)$$

Here, Wrap is the phase wrapping function defined in Eq. (4).

Wrap(θ)

$$= \begin{cases} \tan^{-1}(\sin \theta / \cos \theta) & (\cos \theta \geq 0) \\ \tan^{-1}(\sin \theta / \cos \theta) + \pi & (\cos \theta < 0, \sin \theta \geq 0) \\ \tan^{-1}(\sin \theta / \cos \theta) - \pi & (\cos \theta < 0, \sin \theta < 0) \end{cases} \quad (4)$$

The grating phase θ_g can be obtained as follows:

$$\theta_g = \text{Wrap}(\theta_m + \theta_r). \quad (5)$$

2.2 Phase Analysis of 2D Grating Patterns

Figure 2 shows an x -dimensional phase analysis using the sampling moiré method. Figure 2(a) shows the 2D grating pattern image captured by a CCD camera. Figure 2(b) shows a grating image obtained after the y -dimensional smoothing process. Figure 2(c) shows phase-shifted moiré patterns produced from (b). (d) Phase distribution produced from (c) by the phase-shifting method. (e) Phase distribution of the x -directional reference grating. (f) Phase distribution for the x -directional grating component in the 2D grating image shown in (a). (g) x -directional unwrapped phase distribution.

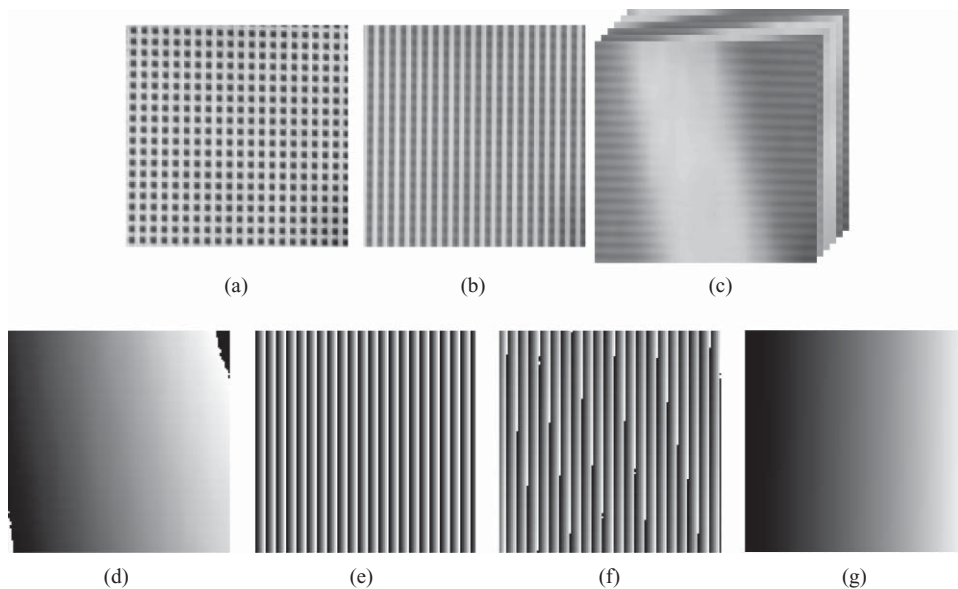


Fig. 2 x -directional phase analysis. (a) 2D grating pattern image captured by a CCD camera. (b) Grating image obtained after the y -dimensional smoothing process. (c) Phase-shifted moiré patterns produced from (b). (d) Phase distribution produced from (c) by the phase-shifting method. (e) Phase distribution of the x -directional reference grating. (f) Phase distribution for the x -directional grating component in the 2D grating image shown in (a). (g) x -directional unwrapped phase distribution.

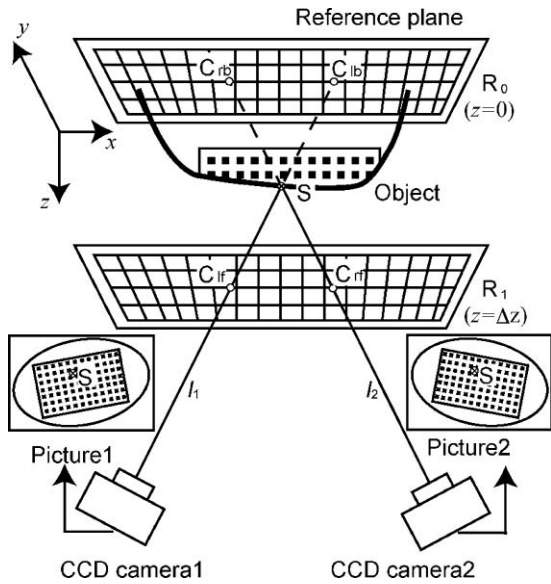


Fig. 3 Arrangement of cameras, reference plane and object.

2D grating is transformed into a 1D grating pattern image. Figure 2(c) shows the phase-shifted moiré patterns produced from Fig. 2(b).

Figure 2(d) shows the phase distribution produced from Fig. 2(c) by the phase-shifting method. Figure 2(e) shows the phase distribution of the *x*-directional reference grating. The period of the reference phase distribution is the same as the pitch of the sampling pixels in the sampling moiré method. Figure 2(e) shows the phase distribution obtained with Eq. (4) for the *x*-directional grating component in the 2D grating image shown in Fig. 2(a). Figure 2(g) shows the *x*-directional unwrapped phase distribution. In the same process, the *y*-dimensional unwrapped phase distribution can be obtained.

3 Principle of Shape and Strain Measurements

3.1 Calibration With Two Reference Planes

Figure 3 shows a schema of the arrangement of cameras, reference planes, and an object. Both the left and right CCD cameras capture the reference planes and the object. In this method, 3D coordinates corresponding to each pixel of the camera are obtained with two reference planes for calibration.

A liquid crystal display is used as the reference plane. The reference plane is placed at two positions, R_0 and R_1 . The reference plane can display grating patterns in the *x*- and *y*-directions with shifting phases. An initial phase for the grating patterns corresponding to each pixel of both cameras can be obtained accurately with a phase-shifting method. The unwrapped phases for the *x* and *y* directions (ϕ_{nx}, ϕ_{ny}) ($n = 0, 1$) are also obtained, with an unwrapping process, at each corresponding pixel of both cameras.

The 3D coordinates (x, y, z) of a point on the reference plane are calculated from the *x* directional grating pitch p_x , the *y*-directional grating pitch p_y , and the *z* position of the reference plane z_n ($n = 0, 1$), as shown in Eq. (5).

$$x = \frac{p_x \phi_{nx}}{2\pi} + x_0, \quad y = \frac{p_y \phi_{ny}}{2\pi} + y_0, \quad z = z_n, \quad (6)$$

Here p_x and p_y are grating pitches for the *x*- and *y*- directions, respectively, and (x_0, y_0) are the coordinates at the point where $(\phi_{nx}, \phi_{ny}) = (0, 0)$. 3D coordinates at a point on the reference plane where the pixel records an image are known for every pixel from each camera. A pixel from each camera has two corresponding points on the two reference planes. A line can be obtained by connecting the two points; that is, a line corresponding to each pixel of each camera can be determined from the results of the calibration method.

3.2 Shape and Strain Distribution Measurements

An object is placed between two reference planes, and the 2D grating attached to the object is captured by the same set of CCD cameras.

Line l_1 passes through point *S* on the object as recorded by CCD camera 1 and line l_2 also passes through point *S* on the object as recorded by CCD camera 2. Line l_1 is the line of sight of a pixel from CCD camera 1 and line l_2 is the line of sight of a pixel from CCD camera 2. Points C_{1b} and C_{1f} are the intersections of line l_1 with reference planes R_0 and R_1 , respectively. Points C_{2b} and C_{2f} are the intersections of line l_2 with reference planes R_0 and R_1 , respectively. The positions of reference planes R_0 and R_1 are $z = 0$ and $z = \Delta z$, respectively. An expression for the straight line l_1 and the straight line l_2 can be obtained from each point C_{1b} , C_{1f} , C_{2b} , and C_{2f} . The 3D coordinates of point *S* are obtained as the intersection of the two lines l_1 and l_2 .

Strain can be calculated from the 3D coordinates of two points, both before and after deformation.

3.3 Finding Corresponding Points

Figure 4 shows the relationship between the 2D grating on an object and the recorded images taken by the left and right cameras. Let us explain how to find corresponding points on the two cameras. Every grating line in the *x*- and *y*-directions has a line number in each direction, and every intersection has its own address, such as (i, j) , composed of the *x*- and *y*-directional line numbers *i* and *j*, respectively. These line numbers increase or decrease sequentially on the surface of the object. Therefore, we are able to sequentially number every grating line on the images. The point on the image whose address is (i, j) is the corresponding point on the surface of the object whose address is (i, j) . Accordingly, correspondence between the image and the object is obtained

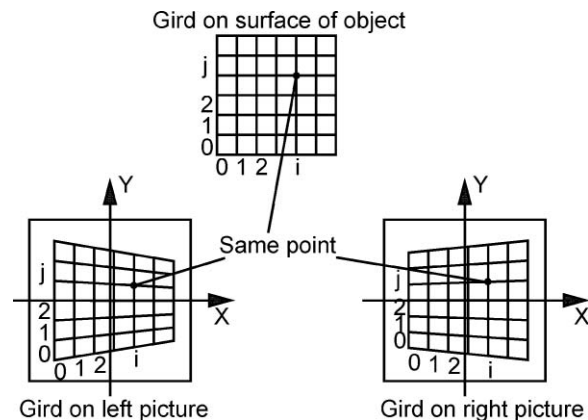


Fig. 4 Relationship between the 2D grating on the object and the images recorded by the left and right cameras.

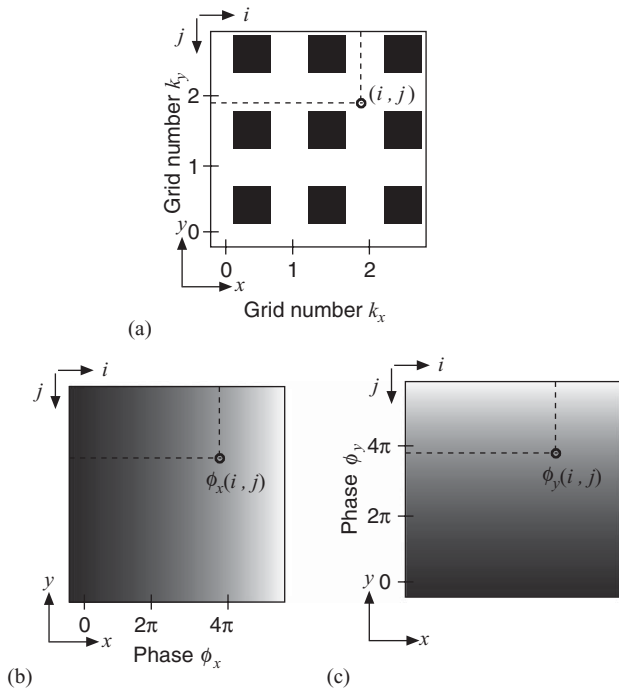


Fig. 5 Relationship between the 2D grating on the object and the phase analyzed image of the x - and y -directions. (a) 2D grating on the object. (b) x -directional unwrapped phase distribution. (c) y -directional unwrapped phase distribution.

by matching the x - and y -directional line numbers on the images.

Figure 5 shows the relationship between the 2D grating on the object and the phase analyzed image of the x - and y -directions. The corresponding points are found from the unwrapped phases (ϕ_x, ϕ_y).

4 Experiments and Results

4.1 Shape Measurement of a Trapezoidal Object

Figure 6 shows an experimental setup for the shape measurement. In this experiment, the accuracy of the shape measurement of the proposed method is confirmed. A trapezoidal object shown in Fig. 7, is placed between reference planes R_0 and R_1 , as shown in Fig. 6. The 2D grating sheet with 2 mm pitches is attached to the specimen as shown in

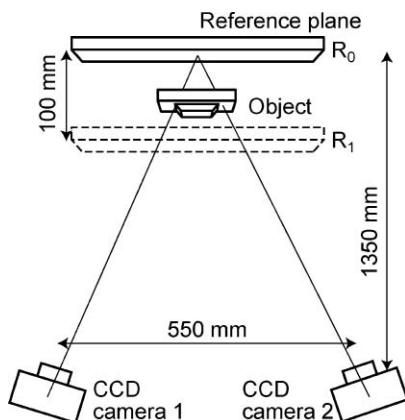


Fig. 6 Experimental setup for the shape measurement.

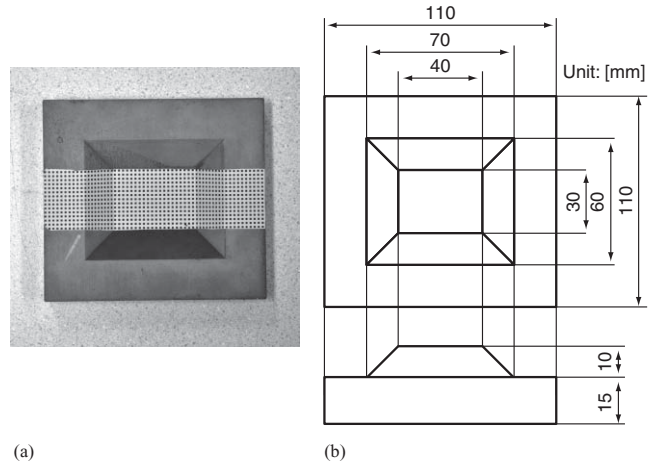


Fig. 7 Specimen of a trapezoidal object; (a) photograph and (b) size of object.

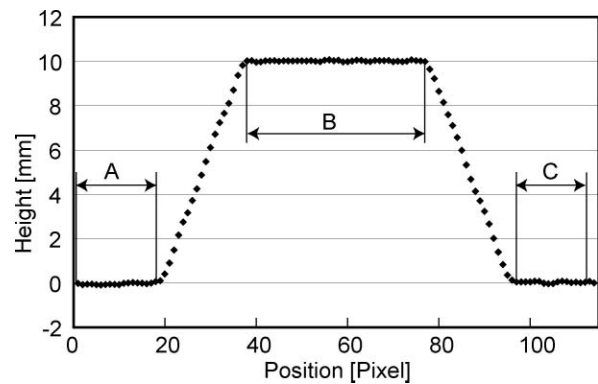


Fig. 8 Result for the shape measurement of the trapezoidal object.

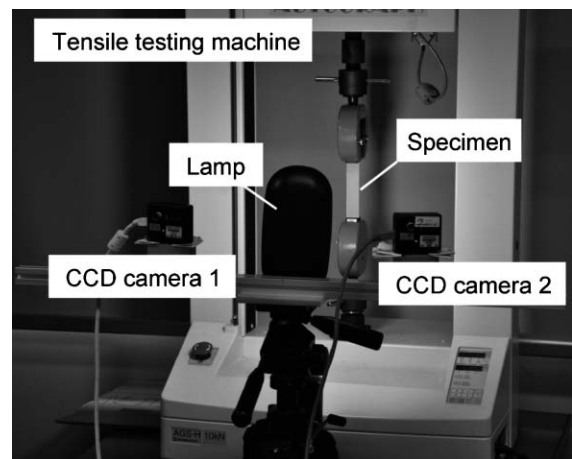


Fig. 9 Experimental setup for the tension test of a stretched rubber belt; (a) Initial state, (b) stretch 5 mm, (c) stretch 10 mm, and (d) stretch 15 mm.

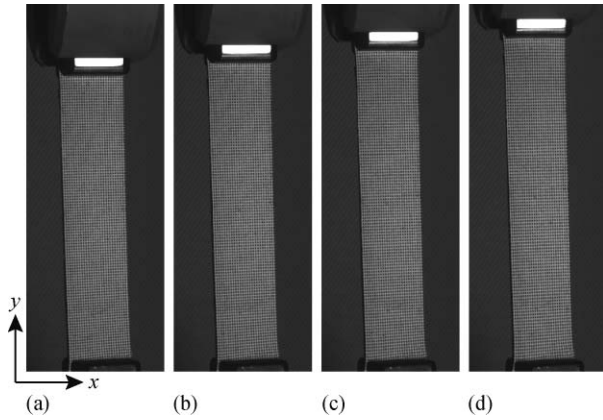


Fig. 10 Specimen images obtained by CCD camera 1.

Fig. 7(a). The distance between two cameras is 550 mm. The distance between the reference plane R_0 and the two cameras is 1350 mm. The distance between the reference planes R_0 and R_1 is 100 mm. The height of the trapezoidal part is 10.00 mm.

Figure 8 shows the result for the shape measurement of the trapezoidal object. Figure 8 shows the contour height distribution along a center position of the trapezoidal object.

The height difference between area A and B is 10.02 mm. The height difference between area B and C is 10.05 mm. The standard deviations of the height values in areas A , B , and C are 0.028, 0.032, and 0.030 mm, respectively.

4.2 Strain Measurement of a Stretched Rubber Belt

Figure 9 shows an experimental setup for a tension test of a stretched rubber belt. In this experiment, the accuracy of the proposed method is confirmed. A rubber plate measuring $25 \times 110 \times 1$ mm is placed on a tensile testing machine. The pitch of the 2D grating attached to the specimen is 1.0 mm.

Figure 10(a) shows an image of the specimen taken by CCD camera 1 in its initial state. The tensile testing machine statically stretches the specimen. Figures 10(b)–10(d) show the specimen stretched 5, 10, and 15 mm, respectively, in the y -direction.

Figures 11(a)–11(f) show the results of the measured strain distribution in the x - and y -directions along the center line of the specimen. Figures 11(a)–11(c) are the x -directional strain distributions when the specimen is stretched in the y -direction by 5, 10, and 15 mm, respectively. Figures 11(d)–11(f) are the y -directional strain distributions when the specimen is stretched in the y -direction by 5, 10, and 15 mm, respectively.

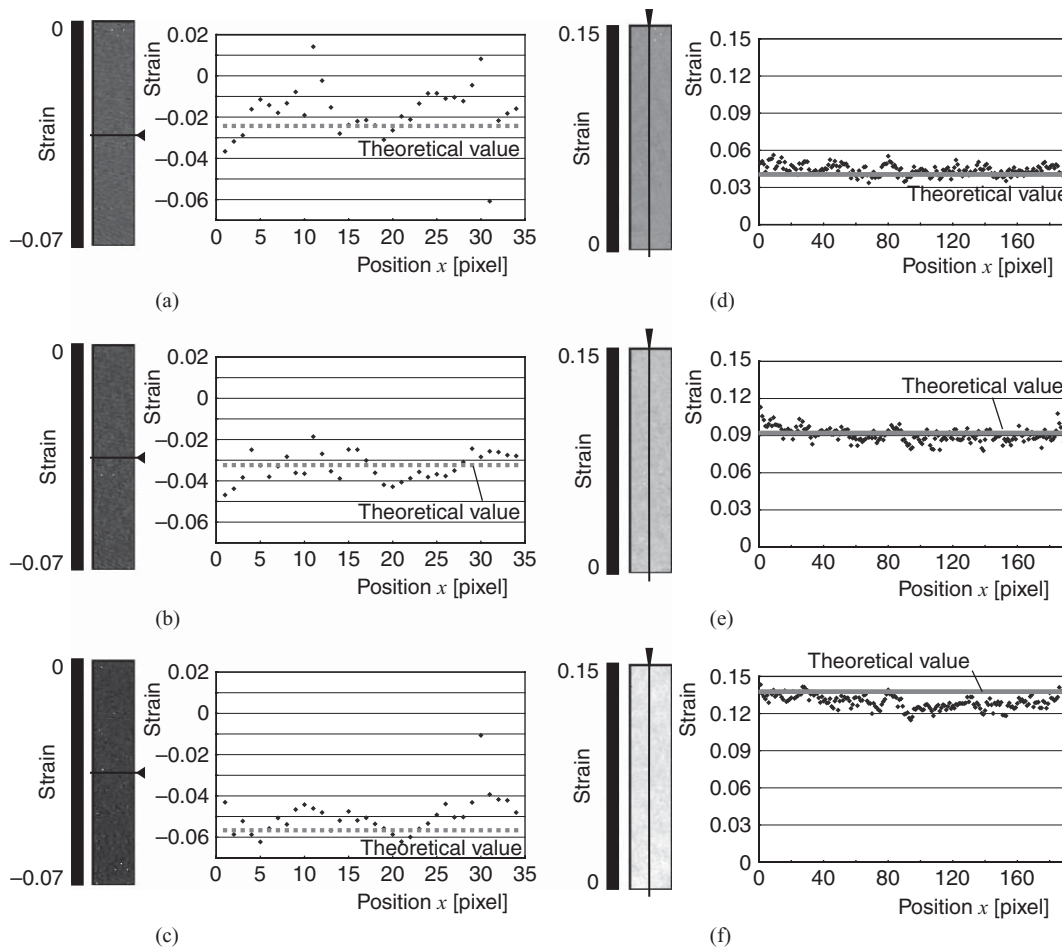


Fig. 11 Results of the measured strain distribution. (a) Strain of stretch 5 mm for x -direction. (b) Strain of stretch 10 mm for x -direction. (c) Strain of stretch 15 mm for x -direction. (d) Strain of stretch 5 mm for y -direction. (e) Strain of stretch 10 mm for y -direction. (f) Strain of stretch 15 mm for y -direction.

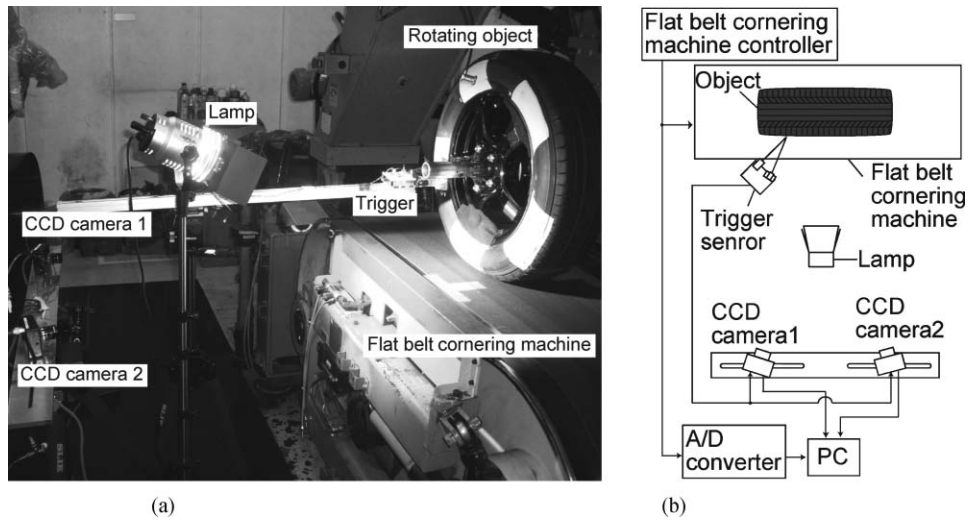


Fig. 12 Experimental setup to measure a rotating tire; (a) photograph and (b) diagram.

The averages of the error between the measured strain and the theoretical strain are -0.007 , 0.001 , 0.007 , -0.004 , 0.001 , and 0.008 in the cases of Figs. 11(a)–11(f), respectively. The standard deviations are 0.013 , 0.007 , 0.009 , 0.004 , 0.006 , and 0.006 in the cases of Figs. 11(a)–11(f), respectively. In this experiment, it was confirmed that this method could be used for the strain measurement of largely deformed objects in materials such as rubber.

4.3 Shape and Strain Measurements of a Rotating Tire

Figure 12 shows the experimental setup. A rotating object is set on a flat belt cornering machine. This test machine can control the rotational speed and the load on the axis. The movement of the flat belt produces the rotation of the object. The rotating object has a 2D grating on its surface, which is a thin rubber sheet. In this experiment, the 2D grating has a 2.0 mm pitch and is printed on the surface of the object, which in this experiment is a tire.

In this experiment, the tire is rotated at 80-km/h (circumferential velocity). Images of the grating are captured by CCD cameras 1 and 2. A trigger signal is produced by a trigger sensor placed behind the object, which detects a white mark attached to the object. CCD cameras 1 and 2 take images simultaneously when the rotating tire triggers the sensor.

The grating image recorded by CCD camera 1 is shown in Fig. 13(a). The phase distribution of the moiré fringe pattern analyzed by the sampling moiré method is shown in Fig. 10(b). The phase distribution of the grating shown in Fig. 13(c) is obtained by using Eq. (1). By unwrapping the phase distribution, the phase distribution is obtained as shown in Fig. 13(d). The image recorded by the right camera is analyzed using the same process.

Figure 14 shows the measurement results of the 3D shape. Figures 15(a)–15(c) show the results of the measured strain

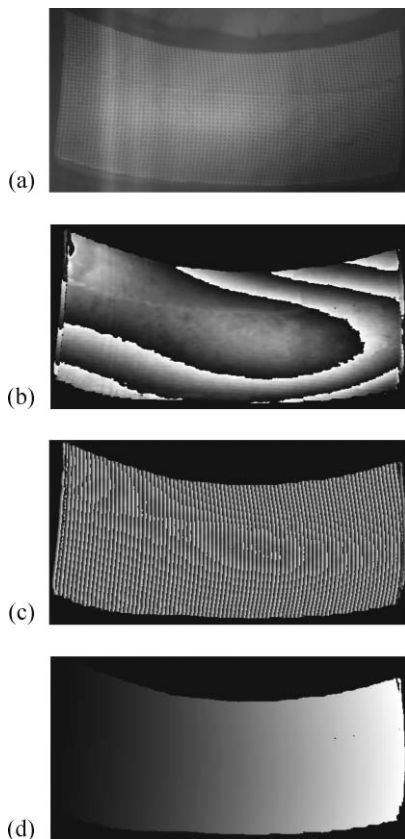


Fig. 13 Phase analysis (in the x-direction); (a) 2D-grating, (b) phase distribution of moiré fringe pattern, (c) phase distribution of the grating, (d) unwrapped phase of the grating.

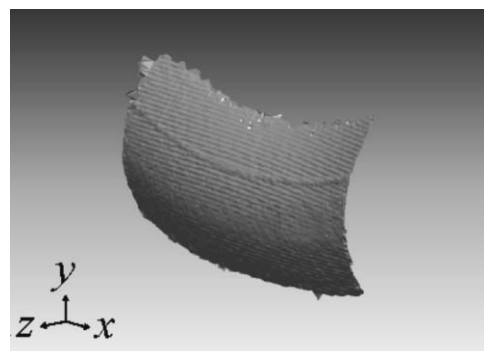


Fig. 14 Measurement result of the 3D shape.

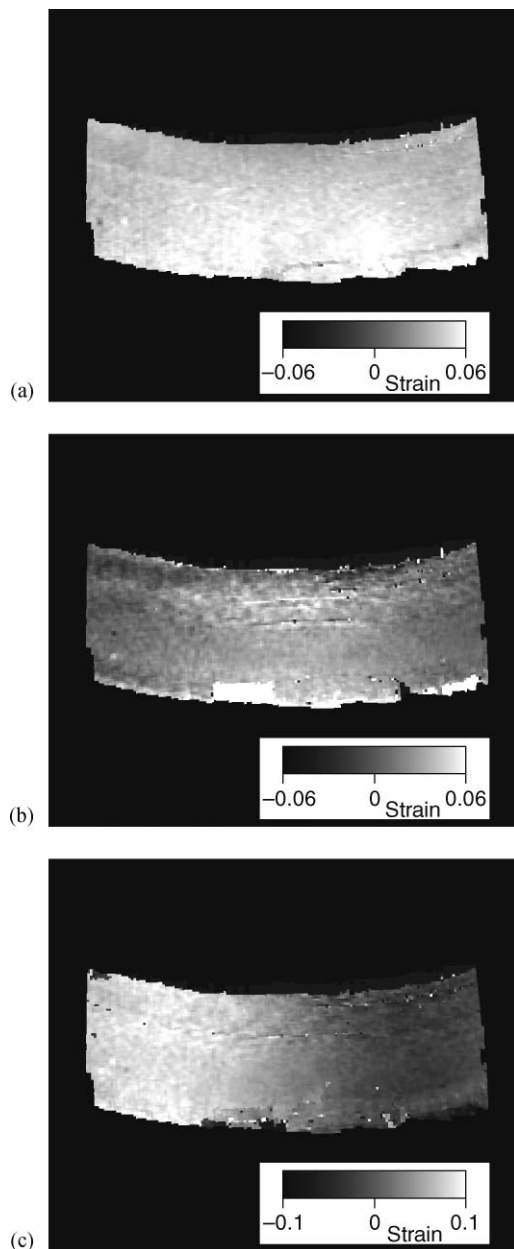


Fig. 15 Measurement results of the strain distributions; (a) strain in the x -direction; (b) strain in the y -direction; and (c) shear strain.

distributions in the x - and y -directions and the shear strain, respectively. In this case, the measured shape when the axis load is 0 is used as the initial shape.

5 Conclusion

In this paper, we developed a shape and strain measurement system using the sampling moiré method for a dynamic moving object such as a tire. First, the accuracy of the shape measurement of the proposed method was confirmed by performing an experiment of a shape measurement of the trapezoidal object. Furthermore, the effectiveness of the strain measurements using this method was also confirmed with an experiment involving a tensile test of a rubber plate. Second, the experimental results of measuring the shape and strain of

a rotating tire are shown. As shown, the 3D shape and strain distribution of a tire rotating at 80 km/h can be accurately measured with this method.

Acknowledgment

We appreciate the cooperation of Dr. Ryoji Hanada and Mr. Hideki Seto in the Yokohama Rubber Company, Ltd. for discussions and experiments.

References

1. H. A. Bruck, S. R. McNeill, M. A. Sutton, and W. H. Peters, "Digital image correlation using Newton-Raphson method of partial differential correction," *Exp. Mech.* **29**(3), 261–267 (1989).
2. S. Yoneyama, A. Kitagawa, K. Kitamura, and H. Kikuta, "In-plane displacement measurement using digital image correlation with lens distortion correction," *JSME International Journal Series A* **49**(3), 458–467 (2006).
3. Y. Motimoto and M. Fujigaki, "Automated analysis of 3-D shape and surface strain distribution of a moving object using stereo vision," *Opt. Laser Eng.* **18**(3), 195–212 (1993).
4. M. Fujigaki, I. H. Yang, and Y. Morimoto, "Strain analysis of moving objects using a Fourier Transform Grid Method," *NDT & E Int.* **29**(4), 197–203 (1996).
5. M. Iwase, "Measurement of tire shape using image processing," *Tire Technology International: The Annual Review of Tire Materials and Tire Manufacturing Technology* 40–43 (1997).
6. Y. Arai, S. Yokozeki, and T. Yamada, "Improvement of spatial fringe analysis method using sampling technique on pixel of CCD," *Jpn. J. Opt.* **24**(9), 581–586 (1995) [in Japanese].
7. Y. Arai, S. Yokozeki, K. Shiraki, and T. Yamada, "High precision two-dimensional spatial fringe analysis method," *J. Mod. Opt.* **44**(4), 739–751 (1997).
8. Y. Arai and S. Yokozeki, "Spatial fringe analysis method in ESPI," *Proc. SPIE* **3744**, 222–230 (1999).
9. Y. Arai and S. Yokozeki, "In-plane displacement measurement using electronic-Speckle-Pattern-Interferometry-Based on spatial fringe analysis method," *Opt. Eng.* **43**(9), 2168–2174 (2004).
10. Y. Arai, H. Hirai, and S. Yokozeki, "Electronic speckle pattern interferometry based on spatial fringe analysis method using two cameras," *J. Mod. Opt.* **55**(2), 281–296 (2008).
11. S. Ri, M. Fujigaki, and Y. Morimoto, "Sampling moiré method for accurate small deformation distribution measurement," *Exp. Mech.* **50**(4), 501–508 (2010).



Motoharu Fujigaki received his BE and ME degrees in mechanical engineering from Osaka University in 1990 and 1992, respectively. He received his doctoral degree from Osaka University in 2001. He worked at NABCO Ltd. from 1992 to 1995. He relocated to Wakayama University in 1995. Currently, he is an associate professor in the Department of Opto-Mechatronics, Faculty of Systems Engineering, Wakayama University. He is interested in optical metrology using image processing, especially shape and deformation measurement using gating projection method and small displacement measurement using laser interferometry. He is a chairperson of the whole-space measurement and inspection consortium. He is a member of SPIE, SEM, OSA, JSEM, JSME, JSNDI, and JSPE.



Kosuke Shimo received his bachelor's degrees in systems engineering from Wakayama University in 2009. Currently, he is a graduate student of Systems Engineering (masters course), Wakayama University. His research interests are shape measurement, strain distribution measurement, and image processing. He is a member of JSEM and JSNDI.



of JSME, JIEP, JSPE, and DBSJ.

Akihiro Masaya received his master's degrees in science and engineering from Ibaraki University in 2007. He was employed with Nakajima Software Engineering Co., Ltd. from 1998 to 2001. He was employed with Hitachi Car Engineering Co., Ltd. from 2001 to 2008. He relocated to Wakayama University in 2008. Currently, he is an assistant professor in Department of Opto-Mechatronics, Faculty of Systems Engineering, Wakayama University. He is a member



ing. His current interests are measurements for shape, deformation, stress, and strain using moiré method and phase-shifting digital holographic interferometry.

Yoshiharu Morimoto graduated master course of Osaka University, Japan in 1968. He is a JSME Fellow and a SEM fellow. He was a member of SEM Executive Board, chairman of ACEM and President of JSEM. He retired from Wakayama University, Japan in 2009 and now he is Professor Emeritus at Wakayama University. He established Moiré Institute Inc. in 2009 and he is now the representative director. His major field of study is experimental mechanics and image processing.